PROCEEDINGS OF SCIENCE

Towards a 3D Neutrino Tomography of the Earth's mantle

Rebekah Pestes,[a,b] **João A. B. Coelho,**[a] **Stéphanie Durand,**[c] **Nobuaki Fuji,**[b,d] **Edouard Kaminski,**[b] **Lukas Maderer**[a] **and Véronique Van Elewyck**[a,d,*]

[a] *Astroparticule et Cosmologie, CNRS, Université Paris Cité, Paris, France*

[b] *Université Paris Cité, Paris, Institut de physique du globe de Paris, CNRS, France*

[c] *Laboratoire de Géologie de Lyon : Terre, Planètes, Environnement, CNRS, UMR 5276, École Normale Supérieure de Lyon, Université de Lyon, Université Claude Bernard Lyon 1*

[d] *Institut Universitaire de France, Paris, France*

E-mail: rpestes@apc.in2p3.fr, nobuaki@ipgp.fr, elewyck@apc.in2p3.fr

Neutrinos can be used to study the interiors of various objects that are difficult to fully probe by classical means. In the case of the Earth, neutrinos provide complementary information to seismic waves because of the imprint of matter effects on their oscillations. This alternative approach may bring new insights on open questions regarding the composition, structure and dynamics of the deep Earth, for example concerning the nature and origin of the large-scale inhomogeneities observed in the lower mantle and known as large low-shear velocity provinces (LLSVPs). In order to be able to explore the potential of present- and future-generation atmospheric neutrino detectors for probing asymmetric models of the Earth's mantle, we extended the capabilities of the OscProb programming library to handle calculating oscillation probabilities for a neutrino trajectory defined by both the zenith and azimuthal angles through an Earth model binned in 3 dimensions: depth, latitude, and longitude. An example using a simplistic model of an LLSVP is provided to demonstrate how this new version of OscProb can be used.

38th International Cosmic Ray Conference (ICRC2023)
26 July - 3 August, 2023
Nagoya, Japan

*Speaker

PoS(ICRC2023)1162

1. Introduction

One of the most powerful tools for imaging the present-day structure of the Earth's interior are seismic waves. They are generated by earthquakes and propagate inside the Earth, probing every layer of it. Their travel times and amplitudes reveal information about the elastic, anelastic and density structure of the Earth. Since the first record of a teleseismic event (Tokyo-Potsdam) in 1889 [1], modern seismology has made tremendous progresses in revealing the 1D [2] and 3D features of the Earth's interior. The averaged depth dependency of the Earth's physical properties, such as density and elasticity, is know to within a few percent [3], and since the 90's, lateral heterogeneity with respect to PREM has been mapped with increasing resolution thanks to the increase in the amount of data as well as in computational power. One of the very first large scale heterogeneities revealed by the 3D seismic imaging of the Earth's mantle are the two large low shear velocity provinces (LLSVPs) that sit at the base of the mantle beneath the Pacific and Africa [4]. They are seen as more or less heterogeneous dome-like structures [5, 6] at which mantle plumes might be anchored [7]. They thus play a critical role in mantle dynamics and Earth's evolution. For instance, they could be a residual of the crystallization of a basal magma ocean [8] or a collection of primordial material brought to the base of the mantle in an early stage of the Earth. There is also the question of their stability through time. All these scenarios could be better discussed if the nature of these LLSVPs, purely thermal or thermo-chemical, were known [9, 10].

A renewed perspective on these questions may come from atmospheric neutrino oscillation tomography, an approach which provides direct sensitivity to the electron density along the neutrino path (see e.g. [11–13] and references therein). The ratio of electron density (N_e) to mass density (ρ_m) scales with the average proton to nucleon ratio (denoted Z/A), which depends on the chemical and isotopic composition of the medium:

$$N_e = (N_A/m_n)(Z/A)\rho_m,$$

where N_A is the Avogadro number and m_n the nucleon mass. With the Z/A ratio being equal to 1 for hydrogen, constraining N_e can be useful to infer information on the distribution of volatile elements in the inner Earth, whose budget is hard to estimate from seismic data because it is challenging to constrain experimentally due to the extreme conditions. Obtaining a 1D/3D N_e distribution inside the Earth, even with low resolution, could therefore help constrain the thermo-chemical evolutionary history of the solid Earth.

2. Simulations with OscProb

OscProb [14] is a C++ programming library, compatible with ROOT [15], that calculates oscillation probabilities for neutrinos traveling through matter, breaking their trajectories into pieces with a constant matter profile. The current implementation of the library relies on a class, called PremModel, that can be used for calculating trajectories going through the Earth, which is particularly useful for simulating atmospheric neutrino oscillation experiments while taking into account the coherent forward scattering of neutrinos with the electrons in the Earth. This class takes a file containing the matter profile for each layer of the Earth, binned in radius, for input and assumes that the Earth is spherically symmetric for the purposes of calculating neutrino trajectories. As a default

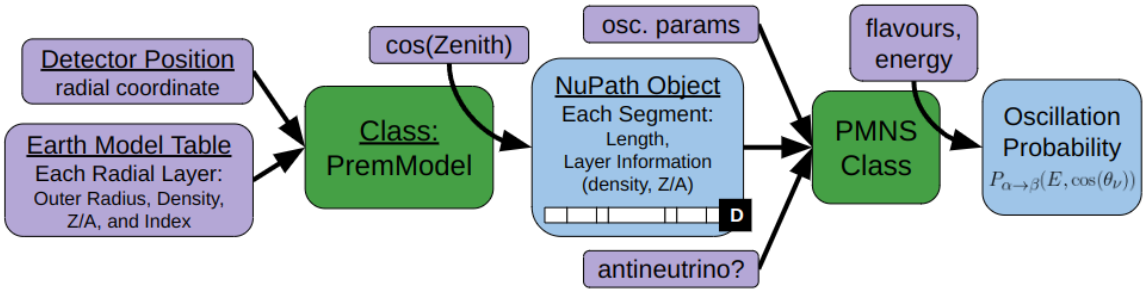

Figure 1: Diagram of the standard workflow for using OscProb. The main classes used are shown in green, the inputs are shown in purple, and the outputs are shown in blue.

Earth model, it uses a density profile based on the Preliminary Reference Earth Model (PREM) [3] with geochemical reservoirs approximated from data in the Geochemical Earth Reference Model (GERM) [16]. The FillPath function within PremModel calculates a neutrino's trajectory, given cosine of the zenith angle, by starting at the location where the neutrino enters the Earth and looping over the radius bins crossed along the way to the detector, using the geometry shown in the left part of figure 2 to find the distance traveled in each bin. This trajectory can then be fed into an object of one of the PMNS classes in order to calculate oscillation probabilities along the path, which completes the standard workflow of OscProb, shown in figure 1.

2.1 Implementation of a 3D Earth Model

In order to allow for lateral inhomogeneities inside the Earth, we needed to augment OscProb with the ability to accept a matter profile that is split up into latitude and longitude bins, in addition to radial bins, and a detector position specified with latitude and longitude, in addition to its radial position. This was done through the creation of a new class, called EarthModelBinned. In order to keep from duplicating code between PremModel and EarthModelBinned, we also created a base class, called EarthModelBase, from which PremModel and EarthModelBinned are derived.

In the EarthModelBinned class, we revamped the FillPath function to fully accommodate the use of a 3D matter profile. In PremModel, only the zenith angle is needed as an argument of FillPath in order to calculate the neutrino's trajectory, but for EarthModelBinned, we added the azimuthal angle (specified as degrees counter-clockwise from North) of the neutrino's trajectory to FillPath's arguments. Now, this FillPath takes these arguments and finds the latitude and longitude where the neutrino with this trajectory enters the Earth. Starting from this point, FillPath loops over the depth bins crossed by the neutrino's trajectory, much like PremModel, checking for latitude and longitude bin crossings before recording the trajectory segment remaining until the next depth bin.

2.1.1 Derivation of equations for bin crossings

In order to calculate where the latitude and longitude bin crossings happen, we first used geometry to find an equation for a vector pointing along the neutrino's trajectory. For a neutrino detected with a zenith angle θ_ν and azimuthal angle ϕ_ν at a detector whose radial, latitude, and longitude coordinates are r_d, θ_d, and ϕ_d, respectively, a unit vector pointing from the detector

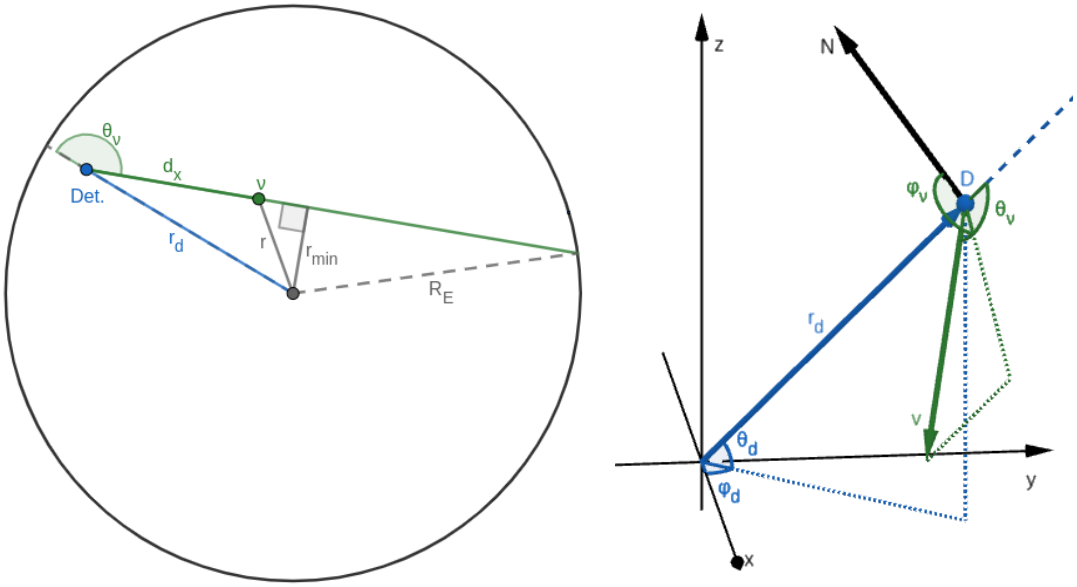

Figure 2: Diagram of a neutrino's trajectory (green) with the detector location (blue) shown in two views: 1) on the left, in a plane through the Earth containing the Earth's center, the detector, and the point at which the neutrino entered the Earth and 2) on the right, as a vector in 3D space.

towards the neutrino's source, as shown in the right part of figure 2, would be

$$\hat{v} = \cos\theta_\nu \hat{r}_d + \sin\theta_\nu \left[\cos\phi_\nu \hat{\theta}_d - \sin\phi_\nu \hat{\phi}_d\right] ,$$

where $\hat{r}_d$ is a unit vector pointing to the detector from the center of the Earth, $\hat{\theta}_d$ is a unit vector pointing north from the detector, and $\hat{\phi}_d$ is a unit vector pointing east from the detector. Using this definition, the vector pointing from the center of the Earth to a point on the trajectory a distance d_x away from the detector is $\vec{x}_\nu = d_x\hat{v} + \vec{r}_d$. The coordinates (in radius r, latitude θ, and longitude ϕ) for this point can then be found with these three equations:

$$r(d_x) = \|\vec{x}_\nu\| , \quad \sin(\theta(d_x)) = \frac{\vec{x}_\nu \cdot \hat{z}}{\|\vec{x}_\nu\|} , \text{ and } \quad \tan(\phi(d_x)) = \frac{\vec{x}_\nu \cdot \hat{y}}{\vec{x}_\nu \cdot \hat{x}} .$$

Putting this all together gives the following for the radial coordinate r, latitude θ, and longitude ϕ:

$$r = \sqrt{r_d^2 + d_x^2 + 2r_d d_x \cos\theta_\nu} , \quad \sin(\theta) = \frac{(r_d + d_x\cos\theta_\nu)\sin\theta_d + d_x \sin\theta_\nu \cos\phi_\nu \cos\theta_d}{\sqrt{r_d^2 + d_x^2 + 2r_d d_x \cos\theta_\nu}} ,$$

$$\text{and } \tan(\phi) = \frac{(r_d + d_x\cos\theta_\nu)\cos\theta_d \sin\phi_d - d_x \sin\theta_\nu (\cos\phi_\nu \sin\theta_d \sin\phi_d + \sin\phi_\nu \cos\phi_d)}{(r_d + d_x\cos\theta_\nu)\cos\theta_d \cos\phi_d - d_x \sin\theta_\nu (\cos\phi_\nu \sin\theta_d \cos\phi_d - \sin\phi_\nu \sin\phi_d)} ,$$

with the signs of the numerator and denominator being used to determine the quadrant of ϕ.

Next, we carefully inverted these equations to come up with expressions for the distance from the detector in terms of each of the coordinates, paying attention to the ranges of variables over which these expressions are valid. From the place where the neutrino enters the Earth, the radial coordinate of the neutrino decreases either until it reaches the detector (for downgoing neutrinos,

Case	Constant	Discontinuity	Initial θ, ϕ
$\sin\theta_\nu = 0$	θ and ϕ	$d_x = r_d$ if $\cos\theta_\nu = -1$	$-\theta_d$, $\phi_d + 180°$
$\sin\phi_\nu = 0$	ϕ	$d_x = \frac{r_d}{\cos\phi_\nu \sin\theta_\nu \tan\theta_d - \cos\theta_\nu}$	$\phi_0 = \phi_d + 180°$
$\cos\theta_d = 0$	ϕ	None	
$\sin\theta_d = 0$ and $\cos\phi_\nu = 0$	θ	None	

Table 1: Special cases noted where the latitude θ and/or longitude ϕ are constant along a neutrino's trajectory, apart from a possible jump discontinuity. The first column defines the case while the other columns specify which variable is constant, where the discontinuity is, and the value of the neutrino's latitude and longitude before reaching the discontinuity, if applicable, while going towards the detector (in all other situations, the value is the same as that of the detector).

i.e. for $\theta_\nu \geq 0$) or until it reaches a minimum given by $r_{\min} = r_d \sin\theta_\nu$ (for upgoing neutrinos, i.e. for $\theta_\nu < 0$). Thus, the equation for d_x in terms of r is

$$d_x(r) = \begin{cases} -r_d\cos\theta_\nu + \sqrt{r^2 - r_d^2\sin^2\theta_\nu} & \text{for } d_x(r) > d_x(r_{\min}) \\ -r_d\cos\theta_\nu - \sqrt{r^2 - r_d^2\sin^2\theta_\nu} & \text{for } d_x(r) < d_x(r_{\min}) \end{cases}, \tag{1}$$

where the two cases are before and after r reaches the minimum value $d_x(r_{\min})$ on the way to the detector, and $d_x(r_{\min}) = -r_d\cos\theta_\nu$ for $\cos\theta_\nu < 0$ and 0 otherwise.

Now, moving on to the latitude and longitude, we noted several special cases that are described in table 1. We designed FillPath to take care of these cases separately as far as finding latitude and longitude bin crossings are concerned.

For all other cases, we used derivatives to characterize the behavior of the latitude and longitude along the neutrino's trajectory in order to specify domains for the inversions to be valid. For the neutrino's latitude, we found that it increases on the way to the detector when $d_x\beta > r_d\cos\phi_\nu\cos\theta_d$, where $\beta \equiv \sin\theta_\nu\sin\theta_d - \cos\theta_\nu\cos\phi_\nu\cos\theta_d$. The only thing in the above inequality that is changing along a single neutrino trajectory is d_x, which is steadily decreasing as the neutrino heads towards the detector. The resulting cases are described in table 2. If $\beta = 0$, then the neutrino's latitude is continually increasing (decreasing) along its trajectory towards the detector for $\cos\phi_\nu < 0$

β	$\cos\phi_\nu$	d_x	latitude	$d_x(\theta)$	s
< 0	anything	$> \frac{r_d\cos\phi_\nu\cos\theta_d}{\beta}$	decreasing	eq. 3	+1
< 0	anything	$< \frac{r_d\cos\phi_\nu\cos\theta_d}{\beta}$	increasing	eq. 3	-1
$= 0$	< 0	anything	increasing	eq. 2	
$= 0$	> 0	anything	decreasing	eq. 2	
> 0	anything	$> \frac{r_d\cos\phi_\nu\cos\theta_d}{\beta}$	increasing	eq. 3	-1
> 0	anything	$< \frac{r_d\cos\phi_\nu\cos\theta_d}{\beta}$	decreasing	eq. 3	+1

Table 2: Scenarios for how latitude θ and distance from the detector d_x are related along a neutrino's trajectory. The first 3 columns are the conditions that define the scenario, and the last 3 columns state how the latitude changes as d_x decreases, which equation is used for $d_x(\theta)$, and what value s has in equation 3, respectively, for each scenario.

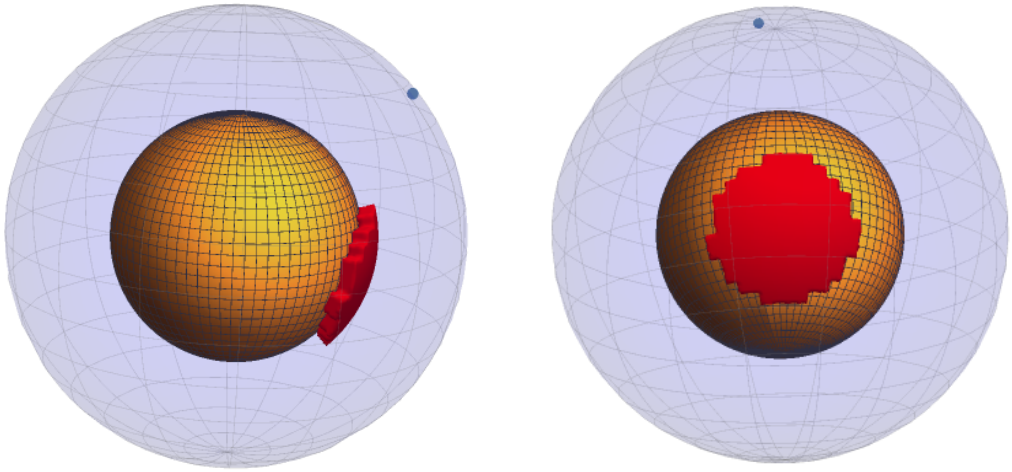

Figure 3: Diagram of the shape and location of the LLSVP (red) in the 3D Earth model used. The Earth's core is shown in yellow with the edges of the latitude and longitude bins on the core's surface shown in black, and the location of the ORCA detector is shown as a blue point.

($\cos\phi_\nu > 0$), and the latitude equation can be easily inverted to find

$$d_x(\theta, \beta = 0) = -r_d \cos\theta_\nu \left[1 + \left(\frac{\sin\theta_\nu \sin\theta}{\sin\theta_d}\right)\left(1 - \frac{\cos^2\theta_\nu \sin^2\theta}{\sin^2\theta_d}\right)^{-1/2}\right] . \tag{2}$$

Otherwise, the inverted equation becomes

$$d_x(\theta, \beta \neq 0) = \begin{cases} \frac{r_d \cos\phi_\nu \cos\theta_d}{\sin\theta_\nu \sin\theta_d - \cos\theta_\nu \cos\phi_\nu \cos\theta_d} - \frac{r_d \sin\theta_d}{\gamma} & \text{for } \sin\theta = \pm\gamma \\ \frac{\cos\theta_\nu \sin^2\theta - \gamma \sin\theta_d + s \sin\theta_\nu \sin\theta \sqrt{\cos^2\theta - \sin^2\phi_\nu \cos^2\theta_d}}{\gamma^2 - \sin^2\theta} r_d & \text{otherwise} \end{cases} , \tag{3}$$

where $\gamma \equiv \sin\theta_\nu \cos\phi_\nu \cos\theta_d + \cos\theta_\nu \sin\theta_d$ and $s = \pm 1$ with the sign being determined from table 2. It may appear that it could be possible for either of the denominators in the $\sin\theta = \pm\gamma$ case of equation 3 to be 0, but in fact, that will not happen outside of the previously addressed scenarios.

For the neutrino's longitude, we found that it is continually increasing (decreasing) along its trajectory on its way to the detector if $\sin\phi_\nu > 0$ ($\sin\phi_\nu < 0$). Thus, the longitude equation can be easily inverted to find

$$d_x(\phi) = \frac{\cos\theta_d \,(\tan\phi_d - \tan\phi)\, r_d}{(\tan\phi_d - \tan\phi)\,\alpha + \sin\theta_\nu \sin\phi_\nu \,(1 + \tan\phi_d \tan\phi)} ,$$

where $\alpha \equiv \sin\theta_\nu \cos\phi_\nu \sin\theta_d - \cos\theta_\nu \cos\theta_d$.

Finally, we used these expressions in FillPath to find at which values of the distance from the detector the neutrino changes latitude, longitude, and radial bins.

3. Outlook

For demonstration purposes, we created a binned 3D Earth model that was identical to the default PremModel, except for having a region that mimics a simplified version of the African

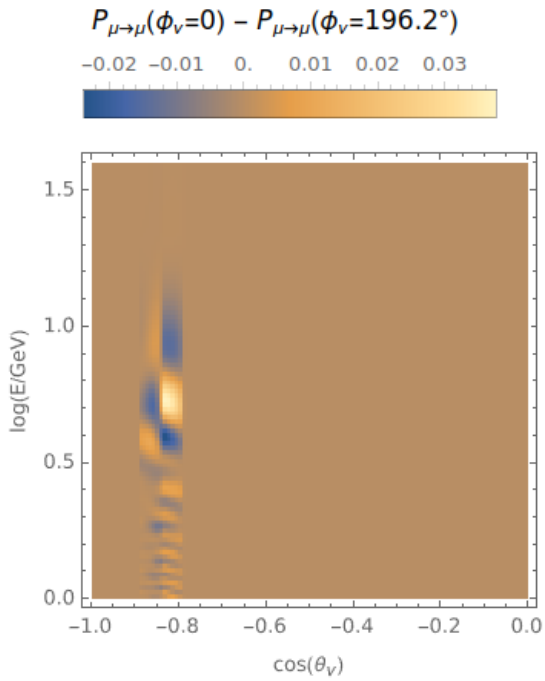

Figure 4: Difference in muon neutrino disappearance probabilities between $\phi_\nu = 0$ and $\phi_\nu = 196.2°$ (which goes through the middle of the LLSVP).

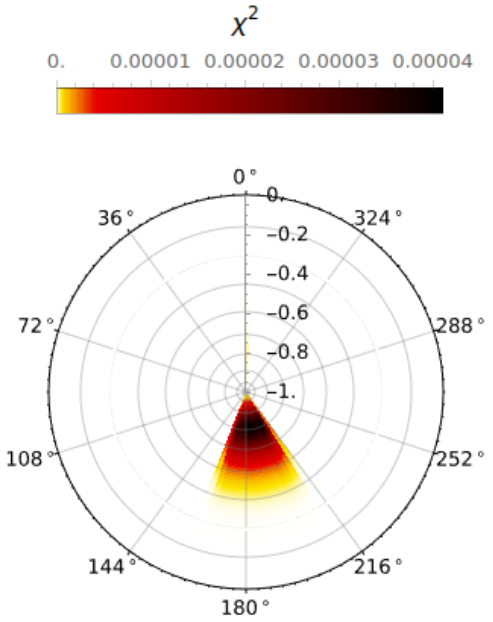

Figure 5: χ^2 plot on a polar ϕ_ν vs $\cos\theta_\nu$ plane, comparing, without marginalization, the expected events in each energy bin with the LLSVP to those without the LLSVP. Smearing is done over the neutrino's energy and zenith angle θ_ν, but not over its azimuthal angle ϕ_ν.

LLSVP, shown in figure 3. The binning of the Earth had 42 radial bins, 36 latitude bins, and 72 longitude bins. For two scenarios of the LLSVP's density (same as PREM and 3% larger than PREM) and a detector with the same location as ORCA, we used OscProb to calculate the oscillation probabilities for 100 values each of the neutrino's energy, zenith angle θ_ν, and azimuthal angle ϕ_ν. A sample of the difference increasing the LLSVP's density by 3% makes is shown in figure 4.

Then, we used the oscillation probabilities calculated with OscProb to determine the expected events in an ORCA-like detector using the same methods and framework as described in [13], augmented to include the azimuthal angle (but without adding in detector resolution effects for the azimuthal angle so far). For each bin (keeping tracks and showers separate), we calculated χ^2 for every bin when fitting the events for the LLSVP case with the events for the case without the LLSVP and did not include minimization over any of the parameters. Finally, we summed the χ^2 values over the energy bins and tracks/showers, plotting the result in figure 5. The "shadow" of the LLSVP can be seen in this plot, but the framework developed now needs to be extended so we can take into account detector effects having to do with the azimuthal angle. With that addition, we can study detector configurations for learning about LLSVPs and other inhomogeneities in the Earth's interior.

Acknowledgements

The authors acknowledge financial support of the LabEx UnivEarthS at Université Paris Cité (ANR-10-LABX-0023 and ANR-18-IDEX-0001)

References

[1] von Rebeur-Paschwitz, E., The earthquake of Tokio, April 18, 1889, Nature, 40 294-295, 1889.

[2] Gutenberg, B., Über Erdbebenwellen, VII A. Beobachtungen an Registrierungen von Fernbeben in Göttingen und Folgerung über die Konstitution des Erdkörpers (mit Tafel), Nachrichten von der Gesellschaft der Wissenschaften zu Göttingen, Mathematisch-Physikalische Klasse, 125-176, 1914.

[3] Dziewonski, A. M. and Anderson, D. L., Preliminary reference Earth model, Physics of the Earth and Planetary Interiors, Volume 25, Issue 4, 1981, Pages 297-356, ISSN 0031-9201, https://doi.org/10.1016/0031-9201(81)90046-7.

[4] Dziewonski, A., B. Hager, and R. O'Connell, Large-scale heterogeneities in the lower mantle, J. Geophys. Res., 82, 239–255, 1977.

[5] French, S.W., Romanowicz, B., Broad plumes rooted at the base of the Earth's mantle beneath major hotspots, Nature, 525, 95-99, 2015.

[6] S. Durand, E. Debayle, Y. Ricard, S. Lambotte, 2016, Seismic evidence for a change in the large-scale tomographic pattern across the D" layer, Geophys. Res. Lett. 43 (15), 7928–7936.

[7] Garnero.J., and McNamara, A. K., Structure and dynamics of Earth's lower mantle. Science. 2008 May 2;320(5876):626-8. doi: 10.1126/science.1148028. PMID: 18451293.

[8] Labrosse, S., J. W. Hernlund, and N. Coltice (2007), A crystallizing dense magma ocean at the base of the Earth's mantle, Nature, 450(7171), 866– 869.

[9] Garnero, J.E., McNamara, A.K., Shim, S.-H., Continent-sized anomalous zones with low seismic velocity at the base of Earth's mantle, Nature geoscience, doi: 10.1038/ngeo2733, 2016.

[10] A.K., McNamara, A review of large low shear velocity provinces and ultra low velocity zones, Tectonophysics, 760, 199-220.

[11] Rott, C., Taketa, A., and Bose, D. (2015). Spectrometry of the earth using neutrino oscillations. Sci. Rep. 5, 15225. doi:10.1038/srep15225

[12] Winter, W. (2016). Atmospheric neutrino oscillations for earth tomography. Nucl. Phys. B908, 250–267. doi:10.1016/j.nuclphysb.2016.03.033

[13] L. Maderer *et al.*, Front. Earth Sci., 14 (2023) Sec. Solid Earth Geophysics Vol. 11 - https://doi.org/10.3389

[14] Coelho, J. A. B., et al. (2023). joaoabcoelho/OscProb: v1.6.1 (v.1.6.1). Zenodo. https://doi.org/10.5281/zenodo.8074017.

[15] Brun R., et al. (2019). root-project/root: v6.18/02 (v6-18-02). Zenodo. https://doi.org/10.5281/zenodo.3895860.

[16] https://earthref.org/GERMRD/datamodel/; McDonough, W.F. (2004). Compositional Model for the Earth's Core. In: Treatise on Geochemistry. Holland, H.D. and Turrekian, K.K. (Editors), Elsevier, Amsterdam, The Netherlands. 2: 547-568; Wedepohl, K.H. (1995). The composition of the continental crust. Geochimica et Cosmochimica Acta 59: 1,217-1,239. doi: 10.1016/0016-7037(95)00038-2; Quinby-Hunt, M.S. and Turekian, K.K. (1983). Distribution of elements in sea water. EOS, Transactions of the American Geophysical Union 64: 130-132; Prinn, R.G. (2004). Ozone, Hydroxyl Radical, and Oxidative Capacity. In: Treatise on Geochemistry. Holland, H.D. and Turekian, K.K. (Editors), Elsevier, Amsterdam. 4: 1-19.